Grid resolution requirement for resolving rare and high intensity wall-shear stress events in direct numerical simulations

Xiang I. A. Yang, Jiarong Hong, Myoungkyu Lee, and Xinyi L. D. Huang

Grid resolution requirement for resolving rare and high intensity wall-shear stress events in direct numerical simulations

Xiang I. A. Yang[1][a], Jiarong Hong[2], Myoungkyu Lee[3], and Xinyi L.D. Huang[1]

[1]Mechanical Engineering, Pennsylvania State University, State College, PA, 16802, USA

[2]Mechanical Engineering, University of Minnesota, Minneapolis, MN 55455

[3]Combustion Research Facility, Sandia National Laboratories, Livermore, CA 94550

Turbulent signals are intermittent with large instantaneous fluctuations. Such large fluctuations lead to small Kolmogorov scales that are hard to resolve in a numerical simulations [Yeung, Sreenivasan, & Pope, *Phys. Rev. Fluids*, 2018, 3, 064603]. The present work follows the above basic logic, but instead of dissipation events in isotropic turbulence, we study wall-shear stress events in plane channel flow. Wall-shear stress fluctuations are increasingly more intermittent as the Reynolds number increases. Hence, one has to employ higher grid resolutions as the Reynolds number increases in order to resolve a given percentage of wall-shear stress events. The objective of this work is to quantify effects of the grid resolutions on the rare and high intensity wall-shear stress events. We find that the standard grid resolution resolves about 99% of the wall-shear stress events at $Re_\tau = 180$. Slightly higher grid resolution has to be employed in order to resolve 99% of the wall-shear stress events at higher Reynolds numbers, and if the standard grid resolution is used for, e.g., a $Re_\tau = 10000$ channel flow, one resolves about 90% to 95% wall-shear stress events.

I. INTRODUCTION

Direct numerical simulation (DNS) gives solutions to the Navier Stokes equation as a function of space and time at a resolution that is usually not possible in a laboratory experiment and therefore is one of the most useful tools for turbulence research [1]. Since the early works of Moser & Moin [2], Kim et al. [3], and Spalart [4], DNS has been extensively used in the studies of wall-bounded flows, and the grid resolution in Ref [3], i.e., $\Delta x^+ \approx 12$, $\Delta z^+ \approx 7$, is considered to be the "standard" DNS grid resolution. (The standard wall-normal grid resolution is $\max[\Delta y^+] \approx 4.5$ at the channel center line and $\min[\Delta y^+] \lesssim 0.1$ at the wall.) Here, x, y, and z are the streamwise, wall-normal, and spanwise directions, and the superscript $+$ denotes normalization by the wall units.

Generally speaking, no simulation is completely error-free [5]—even for DNS. In their seminal work, Kim et al. noted "(there is) not sufficient evidence that the computed (DNS) results are unaffected by the small-scale motions neglected in the computations", calling for more thorough studies of the grid resolution. Oliver et al. [6] assessed the adequacy of the standard DNS grid resolution for channel flow at $Re_\tau = 180$. They concluded that the standard DNS grid resolution is adequate for low-order statistics like the mean flow, the Reynolds shear stresses, and the skin friction coefficient. However, Oliver et al. did not consider rare and high intensity wall-shear stress events, and their discussion was limited to one Reynolds number.

Measuring and predicting wall-shear stress is essential to the study and modeling of wall-bounded flows [7, 8]. The friction velocity, which is determined by the wall-shear stress, appears in many velocity scalings including the logarithmic law of the wall and the scaling of other velocity statistics [9–15]. In the past few years, the fundamental phenomenology of the fluctuating wall-shear stress has received much attention, and DNS has played an important role in unraveling the underlying physics [16–23]. However, without carefully assessing the adequacy of the standard DNS grid resolution, it would be hard to know how much one could trust the conclusions in these studies. From an application standpoint, rare wall shear stress events are responsible for particle entrainment. Hence, accurate modeling of rare wall-shear stress events, or rather, accurate modeling of high-order wall-shear stress statistics, is essential to the numerical modeling of various applications with particle entrainment, e.g., sandstorms, snowdrift, pollen transport, etc. [24–30]

---

[a] xzy48@psu.edu

In this work, we assess the adequacy of the standard DNS grid resolution for rare and high intensity wall-shear stress events. Here, high intensity and rare wall shear stress events are wall shear stress events that are not sufficiently well-resolved by the standard DNS grid resolution. The study will answer the following three questions. First, what must be the grid resolution if we want to resolve the wall layer as well as Kim et al. [3], but at a higher Reynolds number? Second, if we use the same grid resolution as Kim et al. [3], how well is the wall layer resolved at a higher Reynolds number? Third, what wall-shear stress events are missed by the standard DNS grid resolution, but exist in reality? Before we proceed to further motivating the present work, it is worth pointing out that Refs [31, 32] addresses a different question. In Refs [31, 32], the question concerns with the number of grid points needed for a spatially-developing boundary layer given the grid resolution $\Delta x^+ \approx 12$, $\Delta z^+ \approx 7$, whereas the question here concerns with whether the resolution $\Delta x^+ \approx 12$, $\Delta z^+ \approx 7$ is adequate.

The basic logic of this paper generally follows that in Refs [33–37] by Yeung, Sreenivasan, and co-workers. Their basic idea is that large fluctuations in turbulent dissipation lead to small Kolmogorov length scales that require finer-than-standard grids to resolve. For example, a fluctuation in the turbulent dissipation that is $\epsilon = 10000 \langle \epsilon \rangle$ leads to a local instantaneous Kolmogorov scale that is $\eta = 0.1 \left(\nu^3 / \langle \epsilon \rangle \right)^{1/4}$. Here, ϵ is the instantaneous turbulent dissipation, ν is the kinematic viscosity, and $\langle \cdot \rangle$ denotes time averaging. For a DNS whose grid resolution scales with $\overline{\eta} \equiv \left(\nu^3 / \langle \epsilon \rangle \right)^{1/4}$, these events are hard to resolve. The authors then argue that one must use grid resolutions that are increasingly smaller fractions of the Kolmogorov length scale as the Reynolds number increases in order to resolve a given percentage of the dissipation and enstrophy events in isotropic turbulence. The same is true for wall-shear stress fluctuations and DNS of wall-bounded flows. The wall-shear stress in channel flow is increasingly more intermittent as the Reynolds number increases [38] (as evidenced by the increase of wall-shear stress's root-mean-square (rms) as a function of the friction Reynolds number [39, 40]). A large instantaneous fluctuation in the wall-shear stress leads to a small local viscous scale. Hence, one needs grid resolutions that are increasingly smaller multiples of the viscous unit as the friction Reynolds increases in order to resolve a given percentage, say, 99%, of the wall shear stress events in the flow.

In this paper, mulitple DNSs are carried out with refined grids at two friction Reynolds numbers, i.e., $Re_\tau = 180$ and $Re_\tau = 400$, until the resulting probability density function (PDF) of the wall-shear stress is grid converged. We keep our simulations running for an extended period of time to minimize the sampling error [6, 41]. These DNSs allow us to directly assess the adequacy of the standard DNS grid resolution at the two specific Reynolds numbers $Re_\tau = 180$ and 400. Then, we generalize our conclusions to high Reynolds numbers by resorting to known Reynolds number scalings. We show that the standard DNS grid resolution falls short for rare wall-shear stress events. Our conclusion will inevitably cast doubt on some previous studies that relied on DNSs for their study of high intensity and rare wall-shear stress events. However, the objective is not to challenge these authors but to bring a few new thoughts to the discussion.

The rest of the paper is organized as follows. Details of the DNSs are presented in section II. We show the results in section III and discuss their implications. Finally, we summarize in section V following a short discussion in section IV.

II. DNS DETAILS

We conduct a series of incompressible turbulent channel flow DNSs. The flow is periodic in the streamwise (x) and the spanwise (z) directions. No-slip and no-penetration conditions are applied as boundary conditions in the wall-normal (y) direction. For spatial discretization, the code uses the Fourier pseudo-spectral methods in x and z directions and the Chebyshev pseudo-spectral method in y direction [3]. Time-advancement uses the third-order Runge-Kutta. All statistics denoted with "+" in this study are normalized by the combinations of the density, ρ, the kinematic viscosity, ν, and the mean velocity gradient at the wall, $(\partial \langle u \rangle / \partial y |_w)$, where $\langle \cdot \rangle$ denotes the ensemble average. The flow is driven by a constant pressure gradient dP/dx in the x direction.

We consider flows at two Reynolds numbers, i.e., $Re_\tau = 180$ and 400, where Re_τ is the friction Reynolds

TABLE I. DNS Details. The nomenclature of the cases follows the rule of "Resolution"+"Reynolds number". C, R, F, and FF denote "coarse", "regular", "fine", and "finer", respectively. LM180 is the $Re_\tau = 180$ channel flow case in Ref [41]. The size of our computational domain is $L_x \times L_y \times L_z = 4\pi h \times 2h \times 2\pi h$ where h is the channel half width. The domain is larger than the minimal channel [42]. T is the averaging time (after the flow reaches a statistically stationary state). $T_f = L_x/u_b$ is the flow-through time. Here, L_x is streamwise length of the computational domain, and u_b is the bulk velocity.

	Re_τ	Δx^+	Δz^+	Δy^+	T/T_f
C180	180.2	24	13	0.25, 9.4	100
R180	180	12	6.3	0.062, 4.7	100
F180	180.2	5.9	3.1	0.062, 4.7	100
FF180	181.2	2.9	1.6	0.062, 4.7	100
LM180	182.1	4.5	3.1	0.074, 3.2	34.3
C400	399.1	26	14	0.14, 10	100
R400	399.5	12	6.5	0.027, 4.7	100
F400	401.3	5.8	3.3	0.027, 4.7	100
FF400	401.2	2.9	1.8	0.027, 4.7	100

number defined with $u_\tau (= \sqrt{\nu(\partial\langle u\rangle/\partial y)_w})$. Four grid resolutions are considered with successively grid refinements from $\Delta x^+ = 24$, $\Delta z^+ = 13$ to $\Delta x^+ = 2.9$, $\Delta z^+ = 1.6$. The Re_τ of each case varies less than about 0.6% as shown in Table I. Because of the use of a Chebyshev grid, i.e., $y_j = \cos((j-1)\pi/(N_y-1))$, keeping the standard grid resolution at the channel centerline, i.e., $\max[\Delta y^+] \approx 4.7$, results in a wall-grid resolution $\min[\Delta y^+]$ that halves as the Reynolds number doubles. We will show in section IV that further refining wall-normal grid does not affect the wall-shear stress statistics. The time step size is such that the Courant–Friedrichs–Lewy (CFL) number is about 0.8. We follow Ref [6] and average for about $T = 100L_x/u_b$ to minimize sampling errors. We may measure the sampling errors by examining the total stress, i.e., $\nu dU/dy - \langle u'v'\rangle$, of which the analytic solution, $(1 - y/h)u_\tau^2$, is well-known. The deviation of computed total stress from the analytic solution is less than $0.006u_\tau^2$ in all simulation cases. Table I shows the details of our DNSs. The R cases, i.e., R180 and R400, use the standard DNS grid resolution. We include the $Re_\tau = 180$ channel flow data in Ref [41] (denoted with "LM") for comparison, where the grid resolution in the horizontal directions are $\Delta x^+ = 4.5$, $\Delta z^+ = 3.1$, and the distance between B-spline knots in the wall-normal direction gives $\min[\Delta y^+] = 0.074$ and $\max[\Delta y^+] = 3.4$ at the wall and the channel centerline, respectively. Throughout this paper, we use $'$ to denote fluctuation, and σ_ϕ to denote the standard deviation of the quantity ϕ.

III. RESULTS AND DISCUSSION

A. Mean flow and streamwise variance

Figure 1 shows the mean velocity U^+ and the rms of the streamwise velocity fluctuation $u_{\rm rms}^+$. For U^+, the R, F, and FF results collapse, and LM180 agrees well with R180, F180, and FF180. For $u_{\rm rms}^+$, the F and FF results collapse. The R cases predict a slightly smaller peak than the F and FF cases. The LM180 results again agree well with F180 and FF180. For both the mean velocity and the streamwise velocity's rms, the C results are visibly different from the R, F, and FF results. These results are consistent with Ref [6]: the standard DNS grid resolution is sufficient for low-order statistics like the mean flow, the Reynolds stresses, and the skin friction coefficient. In the next subsection, we will examine rare wall-shear stress. Considering that the coarse grid resolution is insufficient for even the low-order statistics like the mean flow, our discussion in the next subsection will focus on the R, F, and FF cases.
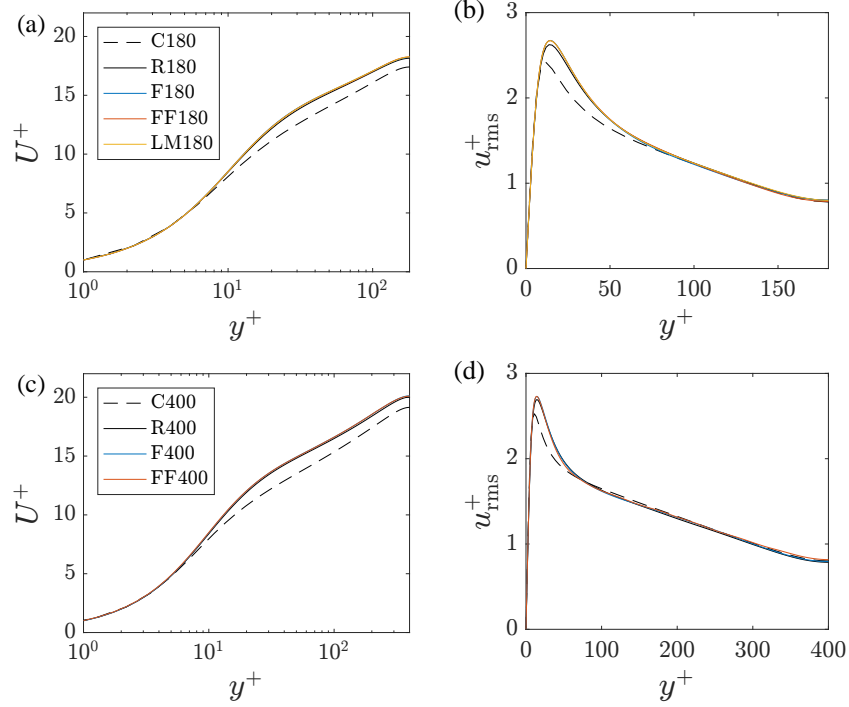
FIG. 1. (a, c) Mean velocity. (b, d) Streamwise velocity's rms. (a, b) Results at $Re_\tau = 180$, (c, d) Results at $Re_\tau = 400$.

B. Wall-shear stress

Figures 2 (a, b) show the PDFs of the streamwise and the spanwise wall-shear stresses in R180, F180, and FF180. Similar to many other turbulent flow quantities, it is more likely to find τ_x and τ_z near their means. ($\langle \tau_x^+ \rangle \equiv 1$ by definition.) These frequent events are not significantly affected by the grid resolution, at least for the three grid resolutions investigated here. In fact, R180, F180, and FF180 predict very similar probability densities near $\tau_x^+ = 1$ and $\tau_z^+ = 0$. The difference between a regular grid, i.e., R180, and a fine grid, i.e., F180 or FF180, arises only at large τ_x and τ_z values. This is consistent with Ref [18, 35, 36], where differences between a coarse grid and a fine grid are found only for rare events, i.e., high dissipation events in Refs. [35, 36] and backflow events in Ref. [18]. For the two quantities in figure 2 (a, b), the R grid leads to higher probability at large τ values than the two fine grids. This is also consistent with Refs [35, 36], where the dissipation rate in an isotropic turbulence DNS is found to be more intermittent on a coarse grid ($\Delta/\eta = 2.22$) than on a fine grid ($\Delta/\eta = 0.55$) at both $Re_\lambda = 390$ and 650, where Re_λ is the Taylor micro scale based Reynolds number.

The results in figure 2 allow us to answer the following question: what percentage of the wall-shear stress events is resolved in R180? To determine that percentage, we draw a horizontal line in figure 2 (a, b) such that the R180 result agrees with the FF180 result above that line. Integrating the probability density function above that horizontal line gives the percentage of the resolved events in R180. In figures 2 (a, b), we draw three lines above which FF180's probability density function integrates to 0.9, 0.99, and 0.999, respectively (i.e., keeping one significant digit for the percentage of the unresolved events). According to figure 2 (a, b), R180 captures between 99% to 99.9% wall-shear stress events. We will be conservative and say that R180 captures 99% of the wall-shear stress events. Now, whether capturing 99% of the wall-shear stress events is sufficient or not depends on the quantity of interest and the desired level of accuracy. Because rare and high intensity events play a more important role in determining higher-order statistics, the level of accuracy we can expect for higher-order statistics like $\langle \tau^4 \rangle$ will be lower than lower-order statistics like $\langle \tau \rangle$. For example,
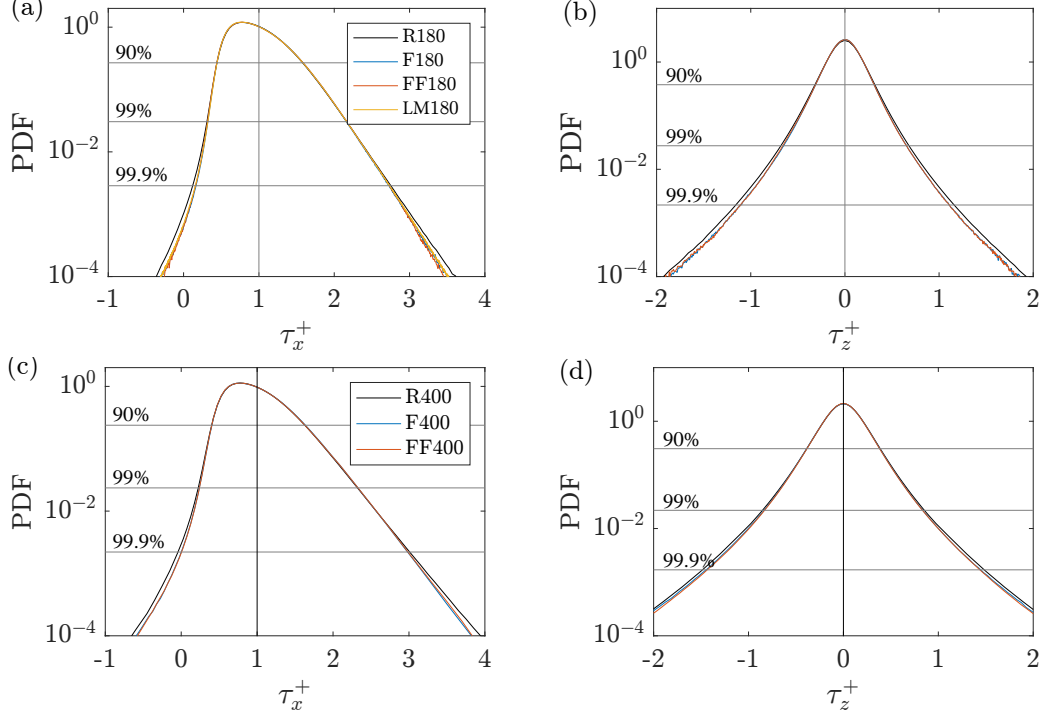
FIG. 2. PDFs of (a) the streamwise wall shear stress and (b) the spanwise wall shear stress in R180, F180, FF180, and LM180. The vertical lines are at $\tau_x^+ = 1$ and $\tau_z^+ = 0$. The horizontal lines are at constant PDF values above which FF180's probability density function integrates to 0.9, 0.99, and 0.999, respectively. (c, d) $Re_\tau = 400$ results.
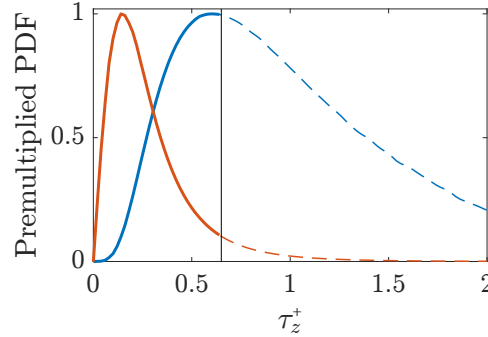

FIG. 3. Normalized premultiplied PDF. R180 Results. Red lines: $\tau_z^+ \times$ PDF. Blue lines: $\tau_z^{+4} \times$ PDF. Solid lines: wall-shear stress events that are resolved in R180. Dashed lines: wall-shear stress events that are not (well) resolved in R180. The premultiplied PDF is symmetric/antisymmetric with respect to $\tau_z^+ = 0$ and we show only the results for $\tau_z^+ > 0$.

let us compute $\langle \tau_z \rangle$, a low-order statistics, and $\langle \tau_z^4 \rangle$, a high order statistics, in R180. Figure 3 shows the premultiplied PDFs $\tau_z^+ \times$ PDF and $\tau_z^{+4} \times$ PDF in R180. The integration of the two premultiplied PDFs gives $\langle \tau_z^+ \rangle$ and $\langle \tau_z^{+4} \rangle$. Following the discussion above, the events $|\tau_z^+| < 0.65$ are well-resolved but the events $|\tau_z^+| > 0.65$ are not. The resolved events are responsible for about 90% of the integration $\int_{\tau_z^+=0}^{\infty}$ PDF $\tau_z^+ d\tau_z^+$ and 30% of the integration $\int_{\tau_z^+=0}^{\infty}$ PDF $\tau_z^{+4} d\tau_z^+$, leading to a much lower level of accuracy for $\langle \tau_z^{+4} \rangle$. The above exercise can be repeated for the $Re_\tau = 400$ results in figure 2 (c, d), and we will arrive at similar conclusions.

Next, we discuss what to expect at higher Reynolds numbers. First, we need to find a scaling that
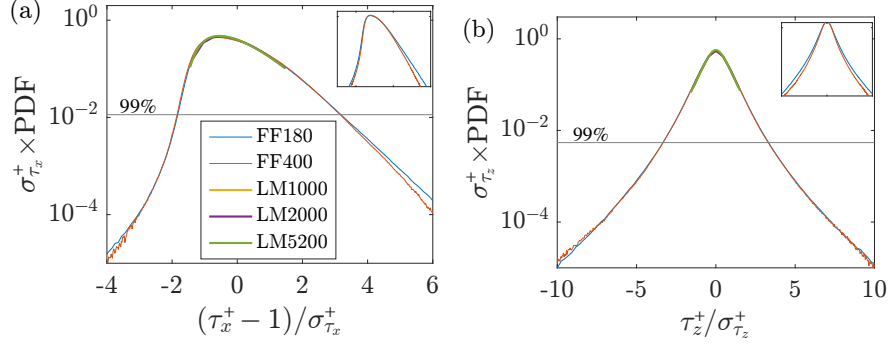
FIG. 4. Scaled PDFs of (a) the streamwise wall shear stress and (b) the spanwise wall shear stress in FF180, FF400, and the channel flow DNSs at $Re_\tau = 1000$, 2000, and 5200 [41]. Details of the LM cases can be found in Ref [41]. As we will show later in this section, the rare events, i.e., the tails of the wall-shear stress PDFs, are not accurately predicted at higher Reynolds number if one uses the standard DNS grid resolution, and therefore the tails of the wall-shear stress PDFs for LM1000, LM2000, and LM5200 are not shown here. The plotted part of the PDFs integrates to 0.9. The two insets are un-scaled PDFs of the streamwise and the spanwise wall-shear stresses for FF180 and FF400. The two horizontal lines are at a constant $\sigma_\tau^+ \times$PDF location above which the PDF integrates to 0.99.

collapses the PDFs of τ_x and τ_z at all Reynolds numbers. According to the previous studies, the scaling $\log(\text{PDF})/\langle\tau'^{+2}\rangle$ $(\tau'^+/\langle\tau'^{+2}\rangle)$ collapse the tails of the PDFs [43] (that is, the tails of the PDFs collapse if one plots $\log(\text{PDF})/\langle\tau'^{+2}\rangle$ as a function of $\tau'^+/\langle\tau'^{+2}\rangle$), and the scaling $\text{PDF}\times\sigma_\tau^+$ (τ'^+/σ_τ^+) collapse the central parts of the PDFs [44]. Here, we need a Reynolds number scaling for the part of the PDF that we can trust, which is the central part of the PDF. Hence, we follow Ref [44] and plot $\text{PDF} \times \sigma_\tau^+$ as a function of τ^+/σ_τ^+. Figure 4 shows the results. We have also included the results at $Re_\tau = 1000$, 2000, and 5200 for comparison purposes. We see from figure 4 that the central parts of the scaled PDFs do collapse. The 99% line intersects with the scaled streamwise wall-shear stress PDF at $(\tau_x^+ - 1)/\sigma_{\tau_x}^+ = -1.9$ and 3.2 and the scaled spanwise wall shear stress PDF at $\tau_z^+/\sigma_{\tau_z}^+ = -3.3$ and 3.3. These are the limiting events for resolving 99% of the wall-shear stress events. In other words, to resolve 99% of the wall-shear stress events, the grid resolution must accommodate the limiting events $(\tau_x^+ - 1)/\sigma_{\tau_x}^+ = 3.2$ and $\tau_z^+/\sigma_{\tau_z}^+ = 3.3$. Here, the Reynolds number information is incorporated in $\sigma_{\tau_x}^+$ and $\sigma_{\tau_z}^+$. In the absence of other length and velocity scales, the resolution needed to resolve a particular wall-shear event τ must be a function of ν and τ, i.e., $\Delta = f(\nu, \tau)$. It follows from the Buckingham π theorem that Δ must be $\Delta x^+ \sim 1/\sqrt{\tau^+}$ and $\Delta z^+ \sim 1/\sqrt{\tau^+}$, i.e., $\Delta x^+ \sqrt{\tau^+} = \text{Constant}$ and $\Delta z^+ \sqrt{\tau^+} = \text{Constant}$. In other words, in order to resolve 99% wall-shear stress events, the grid resolution Δx^+ and Δz^+ must be such that $\Delta x^+ \sqrt{3.2\sigma_{\tau_x}^+ + 1} = C_x$ and $\Delta z^+ \sqrt{3.3\sigma_{\tau_z}^+} = C_z$, where C_x and C_z are two constants. In the above discussion, the fluid density $\rho \equiv 1$ is omitted. We determine the two constants C_x and C_z by plugging in the $\sigma_{\tau_x}^+$ and $\sigma_{\tau_z}^+$ data at $Re_\tau = 180$ and the standard grid resolution (recall that the standard grid resolution resolves 99% wall-shear stress events) and arrive at the following grid resolution requirement

$$\Delta x_{99\%}^+ \approx \frac{18}{\sqrt{3.2\sigma_{\tau_x}^+ + 1}}, \quad \Delta z_{99\%}^+ \approx \frac{5.7}{\sqrt{3.3\sigma_{\tau_z}^+}}, \tag{1}$$

for resolving 99% wall-shear stress events. The number 99% is because R180 resolves 99% of the wall stress events. As both $\sigma_{\tau_x}^+$ and $\sigma_{\tau_z}^+$ are increasing functions of the Reynolds number [39, 40], Δx^+ and Δz^+ in Eq. (1) are decreasing functions of the Reynolds numbers. This is consistent with Refs [35, 36]: one must use resolutions that increasingly smaller fractions of the viscous length scale as the Reynolds number increases in order to resolve a given percentage of the dissipation events.

To get numerical numbers from Eq. (1), we need scaling estimates for $\sigma_{\tau_x}^+$ and $\sigma_{\tau_z}^+$ as a function of the Reynolds number. The exact dependence of $\sigma_{\tau_x}^+$ and $\sigma_{\tau_z}^+$ on the friction Reynolds number Re_τ is not yet well established. For example, Yang et al. [38] argue for
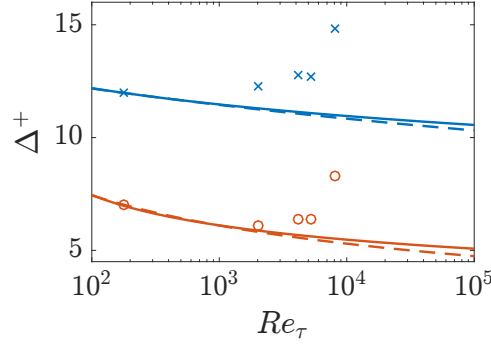
$$\sigma_\tau^{+2} = a\log(Re_\tau) + b, \tag{2}$$

FIG. 5. The grid resolution required to resolve 99% of the wall-shear stress events. Blue lines: Δx^+. Red lines: Δz^+. Solid lines: assuming $\sigma^{+2} \sim \log(Re_\tau)$. Dashed lines: assuming $\sigma^+ \sim \log(Re_\tau)$. Cross symbols: Δx^+ in some of the channel flow DNSs. Round symbols: Δz^+ in some of the channel flow DNSs. The references are: for $Re_\tau = 180$, Ref [3]; for $Re_\tau = 2000$, Ref [41, 49]; for $Re_\tau = 4200$, Ref [42]; for $Re_\tau = 5200$, Ref [41]; and for $Re_\tau = 8000$, Ref [48].

Schlatter et al. [40] argue for

$$\sigma_\tau^+ = a' \log(Re_\tau) + b', \tag{3}$$

and Chen and Sreenivasan [45] argue for

$$\sigma_{\tau_x}^{+2} = a'' \left(0.25 - b'' Re_\tau^{-1/4} \right). \tag{4}$$

The above three scalings all predict an increasing σ_{τ_x} as a function of the Reynolds number, and despite their differences, the three scalings in Eqs. (2), (3), and (4) give very similar predictions at moderately high Reynolds numbers, i.e., for $Re_\tau < O(10^5)$. In addition to the above three scalings that predict an increasing σ_{τ_x} as a function of the Reynolds number, Gubian et al. [46] examined their experimental data and arrived at a somewhat surprising conclusion: σ_{τ_x} stays a constant beyond $Re_\tau \approx 600$. Closely scrutinizing Gubian et al.'s experimental methodology, Örlü and Schlatter [47] later found that the spanwise grooves (spanwise rectangular cavities) that Gubian et al cut on their surfaces to place their hot wires had a big impact on the near-wall flow's dynamics, thereby explaining the somewhat surprising conclusion in Ref. [46]. In this work, we will adopt the more conventional view and rely on the the scalings in Eqs. (2), (3), and (4) that predict an increasing σ_{τ_x} as a function of the Reynolds number. As these three scalings give similar results for DNS's Reynolds number range, we can practically use any one of the three scalings when estimating $\sigma_{\tau_x}^+$ and $\sigma_{\tau_z}^+$. The catch of course is that all these scalings have two undetermined constants that must be fitted to data. Here, we rely on our FF180 and FF400 results to fit for a, b, a', and b' (to give a rough idea of the impacts of using different scalings for σ_τ^+). Substituting Eqs. (2) and (3) in Eq. (1), we have figure 5. We see that the two σ_τ^+ scalings lead to practically the same result. According to figure 5, one only needs to very slightly refine the grid at high Reynolds numbers to resolve as well as Kim et al.'s $Re_\tau = 180$ channel [3]. For example, to resolve 99% of the wall-shear stress events at $Re_\tau = 5200$, one needs $\Delta x^+ = 11$ and $\Delta z^+ = 5.5$, which is slightly finer than the resolution used in Ref [3]. That being said, the present practice has been to use coarser grid at higher Reynolds numbers: Lee & Moser [41] used $\Delta x^+ = 12.7$ for their $Re_\tau = 5200$ channel, Lozano-Duran & Jiminez used $\Delta x^+ = 12.8$ for their $Re_\tau = 4200$ channel, and Yamamoto & Tsuji [48] used $\Delta x^+ = 14.8$ for their $Re_\tau = 8000$ channel (and they use a finite difference code). This is somewhat disconcerting, as we may have been trading off accuracy for higher Reynolds numbers.

The result in figure 5 answers the question: what grid resolution is needed if one wants to resolve the wall layer as well as Kim et al. [3]. Next, we answer the question: how well resolved will the wall layer be at high Reynolds numbers if we use the same grid resolution as Kim et al. [3]? In the above few paragraphs, we come to the conclusion that the standard DNS grid resolution is adequate for the events $\tau_x^+ = 1 + 3.2\, \sigma_{\tau_x}^+ \big|_{Re_\tau=180} = 2.18$, $\tau_z^+ = 3.3\, \sigma_{\tau_z}^+ \big|_{Re_\tau=180} = 0.66$. If one uses the standard DNS grid resolution
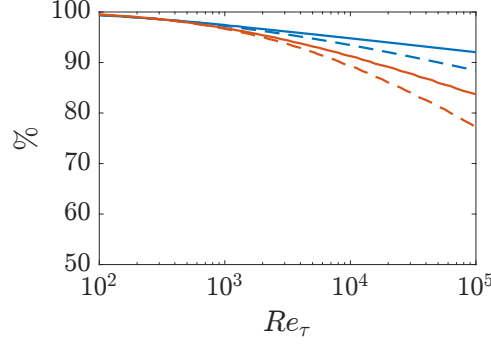
FIG. 6. The percentage of the resolved wall-shear stress events if one uses the standard DNS grid resolution. Blue lines are for streamwise wall-shear stress events. Red lines are for spanwise wall-shear stress events. Solid lines: assuming $\sigma_\tau^{+2} \sim \log(Re_\tau)$. Dashed lines: assuming $\sigma_\tau^+ \sim \log(Re_\tau)$.

at a different Reynolds number, that standard DNS grid resolution should still resolve the events $\tau_x^+ = 2.18$, $\tau_z^+ = 0.66$. Hence, drawing a horizontal line that goes through $\tau_x^+ = 2.18$, i.e., $\tau_x^+/\sigma_{\tau_x}^+ = 2.18/\sigma_{\tau_x}^+$, in figure 4 (a), and $\tau_z^+ = 0.66$, i.e., $\tau_z^+/\sigma_{\tau_z}^+ = 0.66/\sigma_{\tau_z}^+$, in figure 4 (b), and integrating the PDF above the two lines should give the percentage of the resolved wall-shear stress events. Again, the Reynolds number information is embedded in $\sigma_{\tau_x}^+$ and $\sigma_{\tau_z}^+$. That result is shown in figure 6. According to figure 6, if $\sigma_\tau^{+2} \sim \log(Re_\tau)$, the standard DNS grid resolution resolves about 97% of the spanwise wall-shear stress events at $Re_\tau = 1000$ and about 93% of the spanwise wall-shear stress events at $Re_\tau = 5000$. The numbers are not very different if $\sigma_\tau^+ \sim \log(Re_\tau)$. In all, it is safe to say that the standard grid resolution resolves about 90% to 99% of the wall-shear stress events at $Re_\tau = 5000$.

We end this discussion by quoting Kim et al. [3] "(using the standard DNS grid resolution) although the disagreement between the computed and measured values does not seem to be serious, ..., it is important to resolve the differences if the use of the computer-generated databases or experimental data in studying turbulence structures and in developing improved turbulence models is to be continued." Again, the objective of the discussion here is to bring new thoughts to the topic.

C.   Small-scale structures

In this subsection, we answer the last question: what wall-shear stress events are missed by the standard DNS grid resolution that exist in reality? In recent experimental work, Sankar et al. [50] measured the flow in the viscous sublayer. The authors found spanwise meandering motions of fluid parcels at the scale of a few plus units and associated these meandering motions to large spanwise wall-shear stress $|\tau_z|$. The scales of these meandering motions are subgrid for the standard DNS grid resolution, i.e., about 2-3 wall-units in the spanwise direction across a length of 20 wall units in the streamwise direction. Here, we examine if these meandering motions and high spanwise wall-shear stress events are resolved by the standard DNS grid resolution. Figure 7 shows the conditional averaged spanwise wall-shear stress based on $\tau_z^+ > 1.5$ at $x = z = 0$, and we show results for R180, FF180, R400, and FF400. A $\tau_z^+ > 1.5$ event is a rare event. The probability of encountering such an event is less than 0.1% in FF180 and FF400. From figure 7 (a), we see that R180's resolution is obviously insufficient for the $\tau_z^+ > 1.5$ events: the contour lines are symmetric with respect to $z = 0$ in R180 but asymmetric in FF180. Comparing figures 7 (a, b), the difference between the standard DNS grid and the fine grid becomes more notable as the Reynolds number increases, particularly the "streamlines". In all, it is safe to say that the standard DNS grid resolution is insufficient for resolving rare spanwise wall-shear stress events. In this subsection, we have focused on one specific type of wall-shear stress event that we know is not resolved by the standard DNS grid resolution. A more thorough comparison between the R and the FF cases is left to future investigation—when more detailed experimental
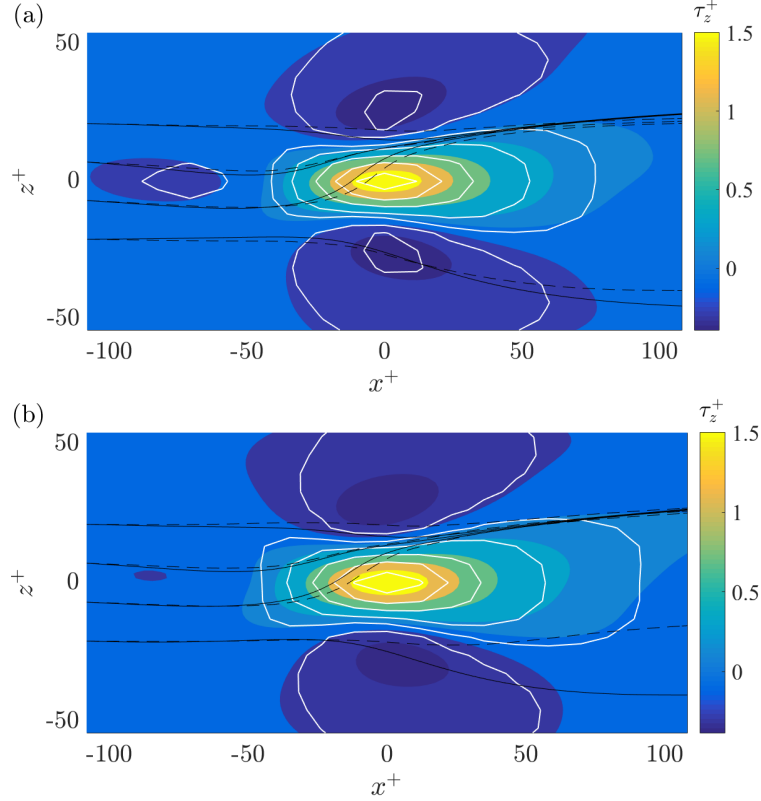
FIG. 7. (a) Conditional averaged the wall-shear stress based on $\tau_z^+ > 1.5$ at $x^+ = z^+ = 0$. The color contour shows the results for FF180. The line contour shows the results for R180. The four black solid lines are streamlines for the vector field (τ_x, τ_z) in FF180. The four dashed solid lines are the results for R180. The solid lines and the dashed lines start at the same x and z locations. (b) Same as (a) but for the results at $Re_\tau = 400$.

measurements of the flow in the viscous sublayer become available.

IV. FURTHER DISCUSSION

When studying rare events in a turbulent flow, one can achieve grid convergence only in a relative sense. In figure 2, cutting off at PDF$> 10^{-4}$, we achieve grid convergence for τ_x and τ_z at the resolution $\Delta x^+ = 5.9$ and $\Delta z^+ = 3.1$. If we were to limit PDF$> 10^{-1}$, we would have achieved grid convergence at the standard resolution $\Delta x^+ = 12$ and $\Delta z^+ = 6.3$. Likewise, if we require grid convergence for, e.g., PDF$> 10^{-7}$, i.e., for very rare events, grid convergence can be achieved only at finer resolutions.

In section II, we discuss the effects of horizontal grid resolutions but not the wall-normal grid resolution. Our code uses a Chebyshev grid in the wall-normal direction. As a result, keeping the standard grid resolution at the channel centerline, i.e., $\max[\Delta y^+] \approx 4.7$ results in a $\min[\Delta y^+]$ that halves as the Reynolds number doubles. The underlying hypothesis of our discussion in section II is that the standard Chebyshev grid is sufficient. Here, we present empirical evidence. Table II shows the details of two additional DNSs: Fy180 and Fy400. Fy180 is F180 but doubling the wall-normal grid number, and Fy400 is F400 but doubling the wall-normal grid. Because of the use of a Chebyshev grid, doubling the number of wall-normal grid quadruples the grid resolution at the wall. Figures 8 (a, b) compare the PDFs of the streamwise and the spanwise wall-shear stresses in F180 and Fy180, and figures 8 (c, d) compare the results in F400 and Fy400. We see that there is barely any difference between the F cases and the Fy cases.

TABLE II. DNS details of the F and the Fy cases.

	Re_τ	Δx^+	Δz^+	Δy^+	T/T_f
F180	180	5.9	3.1	4.7, 0.062	100
Fy180	180	5.9	3.1	2.4, 0.015	100
F400	400	5.8	3.3	4.7, 0.027	100
Fy400	400	5.8	3.3	2.3, 0.0068	100
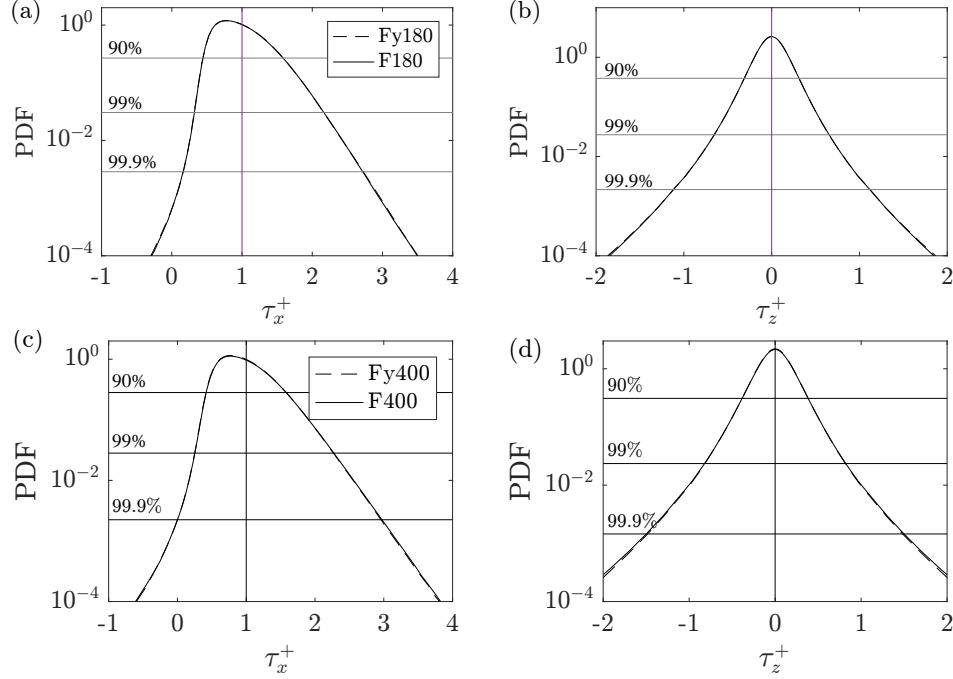
FIG. 8. PDFs of (a) the streamwise wall-shear stress and (b) the spanwise wall-shear stress.

V. CONCLUDING REMARKS

In this work, we conduct channel flow DNSs at two Reynolds numbers, i.e., $Re_\tau = 180$ and $Re_\tau = 400$, and four grid resolutions, i.e., $\Delta x^+ =$24, 12, 5.9, 2.9, and $\Delta z^+ =$13, 6.3, 3.1, 1.6. We show that the standard DNS grid resolution does not capture rare and high intensity wall-shear stress events. Specifically, this work answers the following three questions. First, what grid resolution one needs to use to resolve the wall layer as well as Kim et al.'s $Re_\tau = 180$ DNS [3] but at a higher Reynolds number? Second, how well is the wall layer resolved if one uses the same grid resolution as Kim et al. [3] but at a higher Reynolds number? Third, what wall-shear stress events are not captured by a standard DNS grid but exist in reality? The answers to the above three questions are given in figures 5, 6, and 7. Specifically, we show first that one needs to refine the grid in order to resolve the wall-layer as well as in Ref [3] at a high Reynolds number, second that the wall layer becomes less and less well resolved if one uses the same grid resolution as in Ref [3] for flows at higher and higher Reynolds numbers, and third that the standard DNS grid does not resolve large spanwise wall shear stress events. It is worth noting that by saying "a wall-shear stress event is not well-resolved" we are not saying "a wall-shear stress event does not have the right amount of energy". The two are not the same. For example, one can digitally filter a Gaussian signal such that it has the same energy spectrum as a turbulent signal, but that filtered signal does not resolve any turbulence. When we say "a wall-shear stress event is not well-resolved", we mean that the wall-shear stress event in a simulation is not the same as what it would be in the real world. That being said, wall-shear stress is an intermittent quantity and therefore is

intrinsically hard to resolve.

We conclude our discussion with following remarks. First, our discussion concerns solely with channel flow, but because wall-shear stress in boundary layer flow behaves similarly, conclusions in this paper should still be valid for DNS of boundary layer flow. Second, discretization methods are likely to have a big impact on the results [51]: obviously, lower-order methods will require higher grid resolution than higher-order methods. The conclusions in this work apply to Fourier-Chebyshev spectral codes only. The grid resolution requirement will be much more stringent than the ones suggested in this work if, e.g., a second-order finite difference method is used.

[1] P. Moin and K. Mahesh, "Direct numerical simulation: a tool in turbulence research," *Ann. Rev. Fluid Mech.*, vol. 30, no. 1, pp. 539–578, 1998.

[2] R. D. Moser and P. Moin, "The effects of curvature in wall-bounded turbulent flows," *J. Fluid Mech.*, vol. 175, pp. 479–510, 1987.

[3] J. Kim, P. Moin, and R. D. Moser, "Turbulence statistics in fully developed channel flow at low Reynolds number," *J. Fluid Mech.*, vol. 177, pp. 133–166, 1987.

[4] P. R. Spalart, "Direct simulation of a turbulent boundary layer up to $Re_\theta = 1410$," *J. Fluid Mech.*, vol. 187, pp. 61–98, 1988.

[5] C. J. Roy, "Review of code and solution verification procedures for computational simulation," *J Comput Phys*, vol. 205, no. 1, pp. 131–156, 2005.

[6] T. A. Oliver, N. Malaya, R. Ulerich, and R. D. Moser, "Estimating uncertainties in statistics computed from direct numerical simulation," *Phys. Fluids*, vol. 26, no. 3, p. 035101, 2014.

[7] R. J. Volino and M. P. Schultz, "Determination of wall shear stress from mean velocity and Reynolds shear stress profiles," *Phys. Rev. Fluids*, vol. 3, no. 3, p. 034606, 2018.

[8] Z. Xia, P. Zhang, and X. I. A. Yang, "On skin friction in wall-bounded turbulence," *Acta Mechanica Sinica*, pp. 1–10, 2021.

[9] I. Marusic, J. P. Monty, M. Hultmark, and A. J. Smits, "On the logarithmic region in wall turbulence," *J. Fluid Mech.*, vol. 716, p. R3, 2013.

[10] X. I. A. Yang and M. Abkar, "A hierarchical random additive model for passive scalars in wall-bounded flows at high Reynolds numbers," *J. Fluid Mech.*, vol. 842, p. 354, 2018.

[11] X. I. A. Yang, R. Baidya, Y. Lv, and I. Marusic, "Hierarchical random additive model for the spanwise and wall-normal velocities in wall-bounded flows at high Reynolds numbers," *Phys. Rev. Fluids*, vol. 3, no. 12, p. 124606, 2018.

[12] L.-H. Wang, C.-X. Xu, H. J. Sung, and W.-X. Huang, "Wall-attached structures over a traveling wavy boundary: Turbulent velocity fluctuations," *Phys. Rev. Fluids*, vol. 6, no. 3, p. 034611, 2021.

[13] H. J. Bae and A. Lozano-Durán, "Effect of wall boundary conditions on a wall-modeled large-eddy simulation in a finite-difference framework," *Fluids*, vol. 6, no. 3, p. 112, 2021.

[14] X. Chen, F. Hussain, and Z.-S. She, "Quantifying wall turbulence via a symmetry approach. part 2. Reynolds stresses," *J. Fluid Mech.*, vol. 850, pp. 401–438, 2018.

[15] X. Chen, F. Hussain, and Z.-S. She, "Non-universal scaling transition of momentum cascade in wall turbulence," *J. Fluid Mech.*, vol. 871, 2019.

[16] Z. W. Hu, C. L. Morfey, and N. D. Sandham, "Wall pressure and shear stress spectra from direct simulations of channel flow," *AIAA J.*, vol. 44, no. 7, pp. 1541–1549, 2006.

[17] R. Örlü and P. Schlatter, "On the fluctuating wall-shear stress in zero pressure-gradient turbulent boundary layer flows," *Phys. Fluids*, vol. 23, no. 2, p. 021704, 2011.

[18] P. Lenaers, Q. Li, G. Brethouwer, P. Schlatter, and R. Örlü, "Rare backflow and extreme wall-normal velocity fluctuations in near-wall turbulence," *Phys. Fluids*, vol. 24, no. 3, p. 035110, 2012.

[19] R. Jalalabadi and H. J. Sung, "Influence of backflow on skin friction in turbulent pipe flow," *Phys. Fluids*, vol. 30, no. 6, p. 065104, 2018.

[20] J. I. Cardesa, J. P. Monty, J. Soria, and M. S. Chong, "The structure and dynamics of backflow in turbulent channels," *J. Fluid Mech.*, vol. 880, p. R3, 2019.

[21] M. Lee and R. D. Moser, "Spectral analysis of the budget equation in turbulent channel flows at high reynolds number," *J. Fluid Mech.*, vol. 860, pp. 886–938, 2019.

[22] C. Cheng, W. Li, A. Lozano-Durán, Y. Fan, and H. Liu, "On the structure of streamwise wall-shear stress fluctuations in turbulent channel flows," *J. Phys.*, vol. 1522, no. 1, p. 012010, 2020.

[23] B. Guerrero, M. F. Lambert, and R. C. Chin, "Extreme wall shear stress events in turbulent pipe flows: spatial characteristics of coherent motions," *J. Fluid Mech.*, vol. 904, p. A18, 2020.

[24] J. M. Nelson, R. L. Shreve, S. R. McLean, and T. G. Drake, "Role of near-bed turbulence structure in bed load transport and bed form mechanics," *Water Res. Research*, vol. 31, no. 8, pp. 2071–2086, 1995.

[25] A. Keshavarzy and J. E. Ball, "An application of image processing in the study of sediment motion," *J. Hydraul. Res.*, vol. 37, no. 4, pp. 559–576, 1999.

[26] X. Zheng, *Mechanics of wind-blown sand movements*. Springer Science & Business Media, 2009.

[27] G. Wang and X. Zheng, "Very large scale motions in the atmospheric surface layer: a field investigation," *J. Fluid Mech.*, vol. 802, pp. 464–489, 2016.

[28] P. Wang, S. Feng, X. Zheng, and H. J. Sung, "The scale characteristics and formation mechanism of aeolian sand streamers based on large eddy simulation," *J Geophys Res-Atmos*, vol. 124, no. 21, pp. 11372–11388, 2019.

[29] X. Zheng, T. Jin, and P. Wang, "The influence of surface stress fluctuation on saltation sand transport around threshold," *J Geophys Res-Earth*, vol. 125, no. 5, p. e2019JF005246, 2020.

[30] S. M. Cameron, V. I. Nikora, and M. J. Witz, "Entrainment of sediment particles by very large-scale motions," *J. Fluid Mech.*, vol. 888, p. A7, 2020.

[31] H. Choi and P. Moin, "Grid-point requirements for large eddy simulation: Chapman's estimates revisited," *Phys. Fluids*, vol. 24, no. 1, p. 011702, 2012.

[32] X. I. A. Yang and K. P. Griffin, "Grid-point and time-step requirements for direct numerical simulation and large-eddy simulation," *Phys. Fluids*, vol. 33, no. 1, p. 015108, 2021.

[33] V. Yakhot and K. R. Sreenivasan, "Anomalous scaling of structure functions and dynamic constraints on turbulence simulations," *Journal of statistical physics*, vol. 121, no. 5-6, pp. 823–841, 2005.

[34] J. Schumacher, K. R. Sreenivasan, and P. K. Yeung, "Very fine structures in scalar mixing," *J. Fluid Mech.*, vol. 531, no. 113, 2005.

[35] D. A. Donzis, P. K. Yeung, and K. R. Sreenivasan, "Dissipation and enstrophy in isotropic turbulence: resolution effects and scaling in direct numerical simulations," *Phys. Fluids*, vol. 20, no. 4, p. 045108, 2008.

[36] P. K. Yeung, K. R. Sreenivasan, and S. B. Pope, "Effects of finite spatial and temporal resolution in direct numerical simulations of incompressible isotropic turbulence," *Phys. Rev. Fluids*, vol. 3, no. 6, p. 064603, 2018.

[37] K. Ravikumar, P. K. Yeung, and K. R. Sreenivasan, "Reaching high resolution for studies of intermittency in energy and scalar dissipation rates," *Bulletin of the American Physical Society*, 2020.

[38] X. I. A. Yang and A. Lozano-Durán, "A multifractal model for the momentum transfer process in wall-bounded flows," *J. Fluid Mech.*, vol. 824, p. R2, 2017.

[39] P. H. Alfredsson, A. V. Johansson, J. H. Haritonidis, and H. Eckelmann, "The fluctuating wall-shear stress and the velocity field in the viscous sublayer," *Phys. Fluids*, vol. 31, no. 5, pp. 1026–1033, 1988.

[40] P. Schlatter and R. Örlü, "Assessment of direct numerical simulation data of turbulent boundary layers," *J. Fluid Mech.*, vol. 659, p. 116, 2010.

[41] M. Lee and R. D. Moser, "Direct numerical simulation of turbulent channel flow up to $\mathrm{Re}_\tau = 5200$," *J. Fluid Mech.*, vol. 774, pp. 395–415, 2015.

[42] A. Lozano-Durán and J. Jiménez, "Effect of the computational domain on direct simulations of turbulent channels up to $\mathrm{Re}_\tau = 4200$," *Phys. Fluids*, vol. 26, no. 1, p. 011702, 2014.

[43] M. Ge, X. I. A. Yang, and I. Marusic, "Velocity probability distribution scaling in wall-bounded flows at high

Reynolds numbers," *Phys. Rev. Fluids*, vol. 4, no. 3, p. 034101, 2019.

[44] B. Lindgren, A. V. Johansson, and Y. Tsuji, "Universality of probability density distributions in the overlap region in high Reynolds number turbulent boundary layers," *Phys. Fluids*, vol. 16, no. 7, pp. 2587–2591, 2004.

[45] X. Chen and K. R. Sreenivasan, "Reynolds number scaling of the peak turbulence intensity in wall flows," *J. Fluid Mech.*, vol. 908, p. R3, 2021.

[46] P.-A. Gubian, J. Stoker, J. Medvescek, L. Mydlarski, and B. R. Baliga, "Evolution of wall shear stress with Reynolds number in fully developed turbulent channel flow experiments," *Physical Review Fluids*, vol. 4, no. 7, p. 074606, 2019.

[47] R. Örlü and P. Schlatter, "Comment on "evolution of wall shear stress with reynolds number in fully developed turbulent channel flow experiments"," *Phys. Rev. Fluids*, vol. 5, no. 12, p. 127601, 2020.

[48] Y. Yamamoto and Y. Tsuji, "Numerical evidence of logarithmic regions in channel flow at $\mathrm{Re}_\tau = 8000$," *Phys. Rev. Fluids*, vol. 3, no. 1, p. 012602, 2018.

[49] S. Hoyas and J. Jiménez, "Scaling of the velocity fluctuations in turbulent channels up to $\mathrm{Re}_\tau = 2003$," *Phys. Fluids*, vol. 18, no. 1, p. 011702, 2006.

[50] S. K. Sankar, X. Huang, X. I. A. Yang, and J. Hong, "Meandering motions within the viscous sublayer," *arXiv preprint arXiv:2010.06689*, 2020.

[51] A. W. Vreman and J. G. M. Kuerten, "Comparison of direct numerical simulation databases of turbulent channel flow at $\mathrm{Re}_\tau = 180$," *Phys. Fluids*, vol. 26, no. 1, p. 015102, 2014.